On-chip manipulation of single microparticles, cells, and organisms using surface acoustic waves

Xiaoyun Ding[a], Sz-Chin Steven Lin[a], Brian Kiraly[a], Hongjun Yue[b], Sixing Li[c], I-Kao Chiang[a], Jinjie Shi[a], Stephen J. Benkovic[b,1], and Tony Jun Huang[a,c,1]

[a]Department of Engineering Science and Mechanics, The Pennsylvania State University, University Park, PA 16802; [b]Department of Chemistry, The Pennsylvania State University, University Park, PA 16802; and [c]Cell and Developmental Biology Program, The Pennsylvania State University, University Park, PA 16802

Contributed by Stephen J. Benkovic, June 4, 2012 (sent for review March 12, 2012)

Techniques that can dexterously manipulate single particles, cells, and organisms are invaluable for many applications in biology, chemistry, engineering, and physics. Here, we demonstrate standing surface acoustic wave based "acoustic tweezers" that can trap and manipulate single microparticles, cells, and entire organisms (i.e., *Caenorhabditis elegans*) in a single-layer microfluidic chip. Our acoustic tweezers utilize the wide resonance band of chirped interdigital transducers to achieve real-time control of a standing surface acoustic wave field, which enables flexible manipulation of most known microparticles. The power density required by our acoustic device is significantly lower than its optical counterparts (10,000,000 times less than optical tweezers and 100 times less than optoelectronic tweezers), which renders the technique more biocompatible and amenable to miniaturization. Cell-viability tests were conducted to verify the tweezers' compatibility with biological objects. With its advantages in biocompatibility, miniaturization, and versatility, the acoustic tweezers presented here will become a powerful tool for many disciplines of science and engineering.

C. elegans manipulation | cell manipulation | microfluidics | lab on a chip

Cellular-scale manipulation is essential to many fundamental biomedical studies. For example, the ability to precisely control the physical location of a cell facilitates the investigation of cell—cell and cell—environment interactions (1). Manipulation techniques could also provide tools to help researchers observe the behavior of entire organisms such as *Caenorhabditis elegans* (2, 3). Additionally, these techniques might also aid in molecular dynamics/mechanics studies by allowing researchers to precisely monitor and control the interactions between biomolecules.

Trapping and manipulating microparticles was first demonstrated via optical techniques in 1986, when Arthur Ashkin, Steven Chu, and colleagues first demonstrated trapping of single micrometer-sized dielectric particles with a laser beam, a method now commonly known as optical tweezers (4). Optical tweezers have since been used to trap and manipulate many kinds of micro/nano objects, including dielectric spheres, metal particles, cells, bacteria, DNA, viruses, and molecular motors (5–7). Although optical tweezers have demonstrated excellent precision and versatility for a number of functionalities, they have two potential shortcomings: First, they may cause physiological damage to cells and other biological objects from potential laser-induced heating, multiphoton absorption in biological materials, and the formation of singlet oxygen (8); and second, they rely on complex, potentially expensive optical setups that are difficult to maintain and miniaturize. Many alternative bioparticle-manipulation techniques (9–22) have since been developed to overcome these shortcomings, however, each technique has its own potential drawbacks. For example, magnetic tweezers (17–19) require targets to be prelabeled with magnetic materials, a procedure that affects cell viability; electrophoresis/dielectrophoresis based methods (9–11, 20–22) are strictly dependent on particle polarizibility and medium conductivity and utilize electrical forces that may adversely affect cell physiology due to current-induced heating and/or direct electric-field interaction (23). In this regard, acoustic-based particle manipulation methods present excellent alternatives (24, 25). Compared to their optical, electrical, or magnetic counterparts, acoustic-based methods are relatively noninvasive to biological objects and work for most microparticles regardless of their optical, electrical, or magnetic properties.

To date, many acoustic-based particle manipulation functions (e.g., focusing, separating, sorting, mixing, and patterning) have been realized (25–43). None of these approaches, however, have achieved the dexterity of optical tweezers; in other words, none of the previous acoustic-based methods are capable of precisely manipulating single microparticles or cells along an arbitrary path in two dimensions. The standing surface acoustic wave (SAW)-based acoustic tweezers presented in this article represent the first acoustic manipulation method to precisely control a single microparticle/cell/organism along an arbitrary path within a single-layer microfluidic channel in two dimensions. In our system, SAWs are generated by interdigital transducers (IDTs) deposited on the surface of a piezoelectric substrate. The use of SAWs allows our device to utilize higher excitation frequencies, which results in finer resolution in terms of particle manipulation compared to bulk acoustic waves (BAWs). Additionally, we demonstrate similar manipulation of biological objects, including cells and entire organisms (*C. elegans*). *C. elegans* is an attractive model organism for many biological and medical studies, mainly because of its relatively small size (approximately 1 mm long), optical transparency, well-mapped neuronal system, diverse repertoire of behavioral outputs, and genetic similarities to vertebrates (2). However, trapping and manipulating *C. elegans* has proven to be difficult and generally involves anesthetics, vacuum, cooling, or direct-contact mechanical procedures (2, 3, 44). To our knowledge, our acoustic tweezers are the first to achieve contact-free, noninvasive, precise manipulation of *C. elegans*.

Results and Discussion

Design and Characterization. The working mechanism and device structure of the acoustic tweezers are illustrated in Fig. 1. A 2.5 × 2.5 mm^2 polydimethylsiloxane (PDMS) channel was bonded to a lithium niobate ($LiNbO_3$) piezoelectric substrate asymmetrically between two orthogonal pairs of chirped IDTs (Figs. S1 and S2). Chirped IDTs have a linear gradient in their finger period (Fig. 1*A*) that allows them to resonate at a wide range of frequencies (45). The chirped IDTs in our experiment have 26 pairs of electrodes with the width of electrode and spacing gap increasing linearly from 25 to 50 μm by an increment of 1 μm. The aperture

Author contributions: X.D. and S.-C.S.L. designed research; X.D. and S.L. performed research; X.D. and S.-C.S.L. analyzed data; and X.D., S.-C.S.L., B.K., H.Y., S.L., I.-K.C., J.S., S.J.B., and T.J.H. wrote the paper.

The authors declare no conflict of interest.

[1]To whom correspondence may be addressed. Email: junhuang@psu.edu or sjb1@psu.edu.

This article contains supporting information online at www.pnas.org/lookup/suppl/doi:10.1073/pnas.1209288109/-/DCSupplemental.

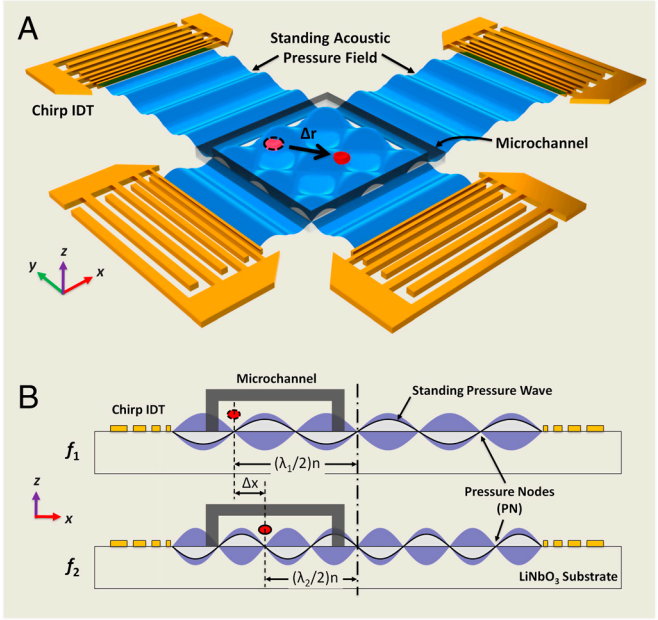

Fig. 1. Device structure and working mechanism of the acoustic tweezers. (*A*) Schematic illustrating a microfluidic device with orthogonal pairs of chirped IDTs for generating standing SAW. An optical image of the device can be seen in Fig. S2. (*B*) A standing SAW field generated by driving chirped IDTs at frequency f_1 and f_2. When particles are trapped at the nth pressure node, they can be translated a distance of $(\Delta\lambda/2)n$ by switching from f_1 to f_2. This relationship indicates that the particle displacement can be tuned by varying the pressure node where the particle is trapped.

of the chirped IDTs is 3.5 mm, larger than the width of the 2.5 × 2.5 mm^2 square channel to ensure full coverage of the standing field. Each pair of chirped IDTs was independently biased with a radiofrequency (rf) signal to generate SAWs; the interference between them forms a standing SAW field on the substrate. The standing SAW leaks into the adjacent fluid medium and establishes a differential pressure field in the fluid; this field generates acoustic radiation forces that act on suspended particles. The acoustic radiation forces drive particles to nodes or antinodes in the acoustic pressure field, depending on their elastic properties (15, 38–43). Most objects, including polystyrene beads, cells, and *C. elegans*, are pushed to the pressure nodes because of density and/or compressibility variations relative to the background medium. The large bandwidth of the chirped IDTs translates into a wide spectrum of accessible standing SAW wavelengths, which defines the large manipulation range of the device. Using chirped IDTs with varying input rf, we can shift the location of the pressure nodes generated from standing SAW interference. As a result, a single particle/cell/*C. elegans* that is trapped in the pressure node can be freely manipulated in two dimensions.

Fig. 1*B* shows a schematic of the standing SAW and related pressure field along one dimension (*x* axis) of the device. We refer to the stationary pressure node in the center of the IDTs as the 0 order node (shown as a long dash dot line in Fig. 1*B*), progressing to the first order, second order, third order, etc. outward from the center. Because absolute node location ($x_n = n\lambda/2$ for n^{th} order pressure node, λ is the SAW wavelength) is directly related to the SAW wavelength, which is dependent on the signal frequency ($f = c/\lambda$, where *c* is the SAW propagation velocity on the surface of substrate), all higher-order ($n > 0$) pressure nodes can be moved simply by altering the applied signal frequency. The node displacement (Δx_n) can be described by: $\Delta x_n = n(\lambda_1 - \lambda_2)/2 = n(c/f_1 - c/f_2)/2$, as shown in Fig. 1*B* for a frequency change from f_1 to f_2. The equation indicates that the particle displacement is directly proportional to the node order.

Fig. 2*A* shows the simulated two-dimensional pressure field surrounding each pressure node, with arrows denoting the acoustic radiation force vectors. The simulation results indicate that a particle between adjacent pressure anti-nodes will experience an attractive force toward the pressure node between them. Fig. 2*B* examines one-dimensional particle motion under varying acoustic power in response to the same frequency shift (also see Movie S1); Fig. 2*C* plots the particle's velocity during this process. At the lower end of the force spectrum (11 dBm, magenta curve in Fig. 2*B* and *C*), a 10-μm fluorescent polystyrene bead can be continuously moved with velocity of approximately 30 μm/s, while at the opposite end of the force spectrum (27 dBm, red

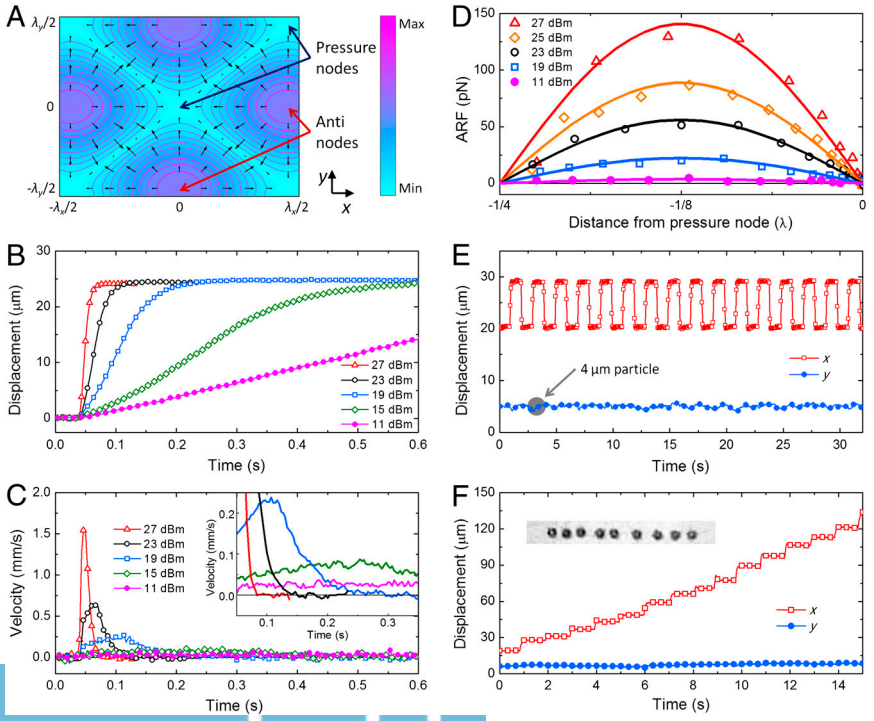

Fig. 2. Quantitative analysis of the acoustic tweezers. (*A*) Simulated pressure field between adjacent pressure anti-nodes. (*B*) One-dimensional particle motion induced by a constant frequency change at varying applied acoustic power (experimental results). (*C*) Velocity plots corresponding to the displacement curves in *B*. *Inset* (smoothed with a moving-average filter of five data points) shows that a velocity of 30 μm/s is achieved at the power input of 11 dBm. (*D*) Experimentally measured acoustic radiation force (ARF) on the particles as a function of distance from the nearest pressure node (discrete points) at different input power levels. The fitted curves are shown in solid lines. (*E*) Demonstration of reproducible particle motion. Here *x*-direction particle motion is repetitively shown between two stationary frequencies to show reproducibility. (*F*) Demonstration of continuous particle translation along the *x* direction in well defined steps, while holding stationary in the *y* direction.

curve in Fig. 2 *B* and *C*), particle velocities as high as approximately 1,600 μm/s are achieved.

We conducted a force analysis to quantitatively determine the magnitude of the acoustic radiation force exerted on the particles at various power inputs. The experimental radiation force is plotted in Fig. 2*D*, calculated from the difference between the drag force (found using the velocity data in Fig. 2*C*) and the time derivative of particle momentum (also calculated from the velocity data in Fig. 2*C*). The force exerted on a 10-μm particle (shown in Fig. 2*D* with discrete points) fits well with the theoretical sinusoidal dependence of the force on the distance to the pressure node (solid lines). Since the acoustic radiation force depends on particle size, compressibility, and standing SAW amplitude, the force exerted on particles (reaching as high as 150 pN for a 10-μm particle) can be predicted and tuned. To demonstrate the stability of our device, the displacement reproducibility is exhibited in Fig. 2*E*, where a 4-μm polystyrene bead is moved back and forth in the *x* direction, while being held stationary in the *y* direction (see Movie S2). The displacement can be reproduced over hundreds of cycles (see Movie S2). Lastly, we repeatedly step a pressure node in the positive *x* direction to demonstrate particle translation over a larger length scale (approximately 100 μm in Fig. 2*F*), again holding the *y* direction constant (also see Movie S3). Fig. 2*F*, *Inset* shows the stacked image of the linear movement of a 10-μm polystyrene bead.

The power density required to manipulate 10-μm polystyrene beads in our setup is approximately 0.5 nW/μm^2 for particle velocities of approximately 30 μm/s, which is much lower than its optical counterparts (10,000,000 times less than optical tweezers and 100 times less than optoelectronic tweezers) (20, 46). The working frequency range of the chirped IDTs used in our setup was 18.5 MHz to 37 MHz, corresponding to SAW wavelengths of approximately 100 μm to 200 μm. The displacement resolution for this device is dependent on the node order and frequency and is theoretically limited by the frequency resolution of the function generator. In our case, imperfect alignment of the PDMS channel and slight frequency fluctuations from the function generator could be responsible for the minor dispersion in the step displacement in Fig. 2*F*. Finally, we note that with the current setup, the acoustic radiation force on objects smaller than 1 μm is theoretically equivalent to the drag force in solution, limiting our current device to microscale objects. Manipulating nano-objects might be possible by using high-frequency SAWs, since the acoustic force is proportional to SAW frequency (15, 41).

Two-Dimensional Manipulation of Single Particles, Cells, and Organisms. To demonstrate single particle/cell manipulation in two dimensions, we tuned the input frequency of both pairs of orthogonally arranged chirped IDTs (as shown in Fig. 1*A*). Each pair of chirped IDTs independently controls particle motion along a single direction, thus the orthogonal arrangement enables complete control in the device plane. The dexterity of this approach is shown in the layered image in Fig. 3*A*, where a 10-μm polystyrene particle is trapped and moved along a path to write "PNAS" (see Movie S4). Fig. 3*B* presents the capture and subsequent manipulation of single bovine red blood cell to trace the letters "PSU" (see Movie S5), demonstrating the applicability of the acoustic technique to biological samples.

To further demonstrate the biocompatible nature of this technique, we conducted HeLa cells viability and proliferation assay after exposure to high-power (23 dBm) standing SAW fields for 6 s, 1 min, and 10 min. The results (see Fig. 4 and *Methods*) indicate that after 10 min in the standing SAW field, no significant physiological damage was found on the cell viability and proliferation. Additional control experiments were conducted to examine the heating effects of our acoustic device on the channel. After 10 min of acoustic power at 23 dBm, the temperature increased from 25 °C to 27.9 °C. For an exposure time of 1 min, the temperature increase was less than 2 °C (see Fig. S3). At a higher input power level (25 dBm), which was required for *C. elegans* manipulation, the temperature was stabilized at 31 °C even after 10 min.

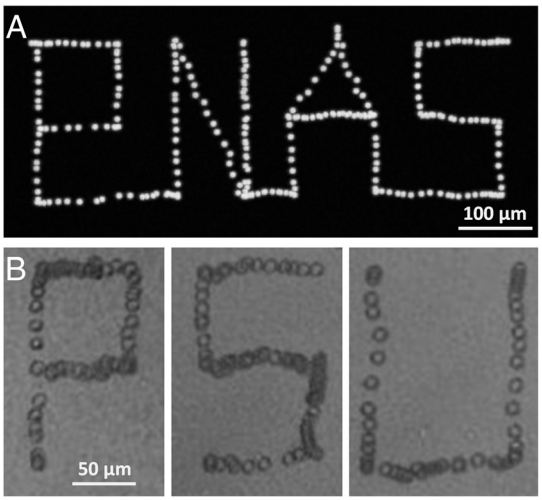

Fig. 3. Independent two-dimensional single particle and cell manipulation. (*A*) Stacked images used to demonstrate independent motion in *x* and *y* using a 10-μm fluorescent polystyrene bead to write the word "PNAS." (*B*) Stacked images showing dynamic control of a bovine red blood cell to trace the letters "PSU." The diameter of bovine red blood cell is about 6 μm.

In addition to microparticles and cells, this acoustic device can also be used to manipulate entire multicellular organisms, such as *C. elegans*. This task is challenging for optical techniques

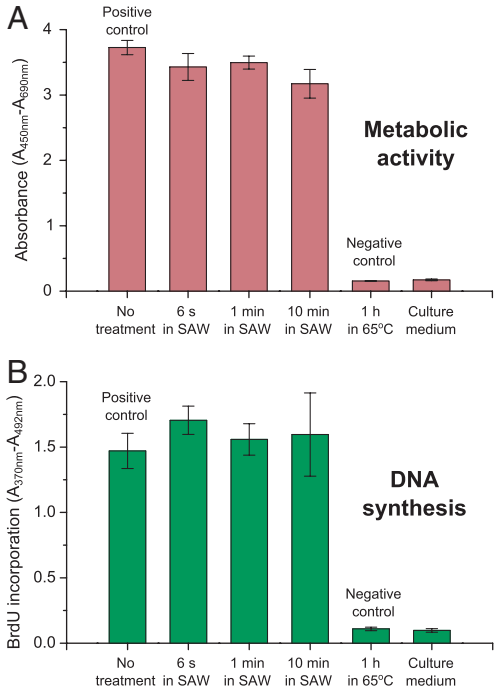

Fig. 4. Experimental results for cell viability and proliferation tests. HeLa cells were incubated for 20 h after being treated in SAW field for 6 s, 1 min, and 10 min, respectively, under the input power of 23 dBm, and then (*A*) metabolic activity was measured at 450 nm after 2 h BrdU labeling and following 2 h reagent WST-1 reincubation, to verify the cell viability. Subsequently, (*B*) DNA synthesis was determined using Cell Proliferation ELISA to verify the cell viability. As control experiments, cells were examined without SAW treatment and at 65 °C for 1 h. The culture medium with no cell was also measured as comparison. Each group was tested five times.

because high power density must be applied over larger areas, leading to impractical total power requirements. Using the same experimental conditions as single cells and particles, we trapped and independently translated *C. elegans* in the *x* and *y* directions (Fig. 5 *A–D*, also see Movie S6). The *C. elegans* was moved in either the *x* or *y* direction when we turned on the power and swept the frequency and returned to normal behavior after the power was shut off. As seen in Fig. 5 *E* and *F*, the *C. elegans* can also be immobilized along their entire length and be stretched in a standing SAW acoustic field. The immobilization and stretching can be maintained for extended periods of time without inducing physiological damage, allowing long-term, full-body studies to be undertaken.

Finally, our acoustic tweezers can also simultaneously manipulate large numbers of particles. Although at this stage the technique cannot select an individual particle from a group, parallel manipulation of multiple particles can be achieved with clusters of particles at a single pressure node, single particles at different pressure nodes, or clusters of particles at distinct pressure nodes. This manipulation can occur over a variety of length scales (see Movies S7 and S8). These videos show that whereas the acoustic tweezers are capable of dynamically manipulating single particles/cells/organisms, they are also capable of simultaneously manipulating more than tens of thousands of particles/cells.

Conclusion

In summary, we have demonstrated standing SAW-based acoustic tweezers that can manipulate single particles/cells/organisms in a microfluidic chip. This acoustic device has significant advantages in biocompatibility and versatility. The lower power density requirement renders our technique extremely safe to biological samples. The simple structure/setup of these acoustic tweezers can be integrated with a small rf power supply and basic electronics to function as a fully integrated, portable, and inexpensive particle-manipulation system. The technique's versatility has three aspects: (1) it is capable of manipulating most microparticles regardless of shape, electrical, magnetic, or optical properties; (2) it is capable of manipulating objects with a variety of length scales, from nanometer (if we use higher SAW frequency) to millimeter (as demonstrated in *C. elegans*); and (3) it is capable of manipulating a single particle or groups of particles (e.g., tens of thousands of particles). The acoustic tweezers' versatility, biocompatibility, and dexterity render them an excellent platform for a wide range of applications in the biological, chemical, and physical sciences, including the fundamental studies of mechanical properties of micro- and nanoscale particles such as cells, DNAs, proteins, and molecules. Additionally, the ability to massively move particles with great speed (up to 1,600 μm/s) could make this technique a key tool in many high-throughput assays such as cell sorting and separation. Finally, this device could be used to help researchers examine the behavioral and neuronal response of small organisms (such as *C. elegans*) to mechanical and chemical stimuli.

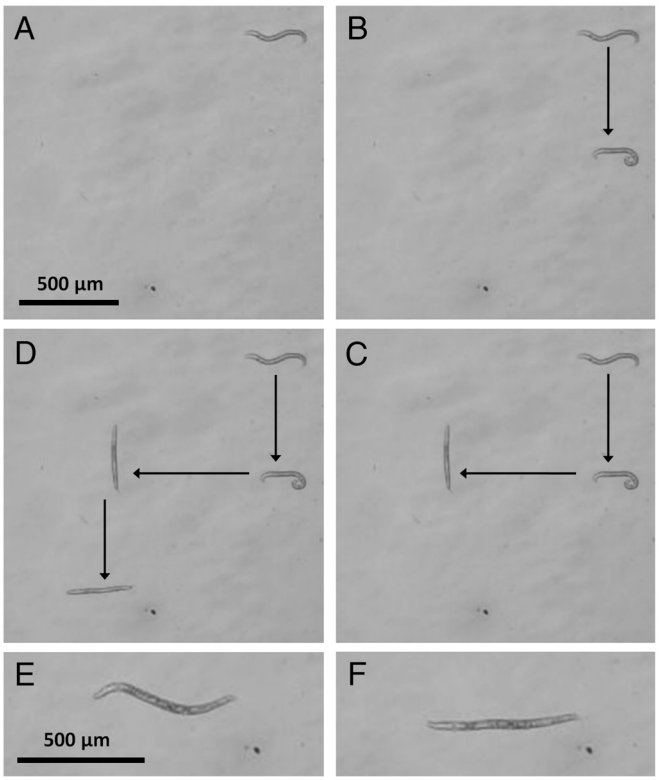

Fig. 5. Single *C. elegans* manipulation. One single *C. elegans* was (*A*) trapped, (*B*) moved in *y* direction, (*C*) moved in *x* direction, and (*D*) moved in *y* direction again and released, with the average velocity of approximately 40 μm/s. An optical image of *C. elegans* (*E*) before and (*F*) after being fully stretched.

Methods

Experimental Setup. A 2.5 × 2.5 mm^2 PDMS channel was bonded to a $LiNbO_3$ piezoelectric substrate asymmetrically between two orthogonal pairs of chirped IDTs, to form the acoustic device. Two major steps were involved in the fabrication: (1) the fabrication of chirped IDTs, and (2) the fabrication of PDMS microchannel (see *SI Text* for more details). The manipulation device was mounted on the stage of an inverted microscope (Nikon TE2000U). Two rf signals were generated from two function generators (Agilent E4422B) to drive the two pairs of chirped IDTs independently. Solutions of bovine red blood cells (approximately 6 μm in diameter, Innovative Research, Inc.), *C. elegans*, or fluorescent polystyrene beads with diameters of 2, 4, 7, 10, and 15 μm were injected into the channel before the rf signals were applied. A CCD camera (CoolSNAP HQ2, Photometrics,) and a fast camera (Casio EX-F1) were connected to the microscope to capture the manipulation process.

Cell Viability and Proliferation Assays. HeLa cell viability and proliferation tests were conducted through the measurements of metabolic activity and DNA synthesis to further exam the noninvasiveness of our technique (37). HeLa cells were incubated in Dulbecco's modified Eagle medium (DMEM)-F12 medium (Gibco), with 10% fetal bovine serum (Atlanta Biologicals), penicillin (100 U/mL), and 100 μg/mL streptomycin (Mediatech) to about 90% confluence before trypsinization (Trypsin + 0.05% EDTA, Gibco) and dilution to 2×10^5 cells/mL in medium. We treated 100 μL HeLa cell suspensions in five different conditions, respectively: (1) untreated cells (positive control); under SAW radiation for (2) 6 s; (3) 1 min; (4) 10 min; and (5) at 65 °C for 1 h (negative control). After treatment, HeLa cells were seeded into Costar 96-well black clear-bottom plate (Corning Life Sciences) with seeding density of 2×10^4 cells/well in 100 μL culture medium. 100 μL fresh medium was added into separate well as blank control. Cells were then incubated for 20 h after which we added 10 μL/well BrdU labeling solution (Roche Applied Science). After labeling for 2 h we added 10 μL/well water-soluble tetrazolium salts (WST-1; Roche Applied Science) and reincubated for another 2 h. Then we measured absorbance of each well at 450 and 690 nm (reference) with an absorbance reader (BioTek). Subsequently, BrdU incorporation was determined with Cell Proliferation ELISA, BrdU (colorimetric) (Roche Applied Science) and the absorbance of each well at 370 and 492 nm (reference) was measured with the absorbance reader. Five separate studies were conducted for each condition under input power of 23 dBm, and the averages were given. The results were tallied in Fig. 4.

ACKNOWLEDGMENTS. We thank Dr. Bernhard R. Tittmann and Brian Reinhardt for assistance with equipment, Dr. Vivek Kapur for the assistance with cells viability and proliferation assay, and Dr. Craig E. Cameron for providing cultured HeLa cells and Dr. Wendy Hanna-Rose for providing cultured *C. elegans* for our experiments. We also thank Dr. Vincent H. Crespi, Daniel Ahmed, Michael Lapsley, Dr. Danqi Chen, Dr. Xiaole Mao, and Dr. Yanjun Liu for helpful discussion. This research was supported by National Institutes of Health Director's New Innovator Award (1DP2OD007209-01), National Science Foundation (NSF) (1102206), NSF Graduate Research Fellowship (Grant No. DGE-0750756), and the Penn State Center for Nanoscale Science (MRSEC). Components of this work were conducted at the Penn State node of the NSF-funded National Nanotechnology Infrastructure Network.

1. Hui EE, Bhatia SN (2007) Micromechanical control of cell–cell interactions. *Proc Natl Acad Sci USA* 104:5722–5726.
2. Chronis N, Zimmer M, Bargmann CI (2007) Microfluidics for in vivo imaging of neuronal and behavioral activity in *Caenorhabditis elegans*. *Nat Methods* 4:727–731.
3. Rohde CB, Zeng F, Gonzalez-Rubio R, Angel M, Yanik MF (2007) Microfluidic system for on-chip high-throughput whole-animal sorting and screening at subcellular resolution. *Proc Natl Acad Sci USA* 104:13891–13895.
4. Ashkin A, Dziedzic JM, Bjorkholm JE, Chu S (1986) Observation of a single-beam gradient force optical trap for dielectric particles. *Opt Lett* 11:288–290.
5. Grier DG (2003) A revolution in optical manipulation. *Nature* 424:810–816.
6. Zhang X, Halvorsen K, Zhang CZ, Wong WP, Springer TA (2009) Mechanoenzymatic cleavage of the ultralarge vascular protein von Willebrand factor. *Science* 324:1330–1334.
7. Yang AHJ, et al. (2009) Optical manipulation of nanoparticles and biomolecules in sub-wavelength slot waveguides. *Nature* 457:71–75.
8. Rasmussen MB, Oddershede LB, Siegumfeldt H (2008) Optical tweezers cause physiological damage to *Escherichia coli* and *Listeria* bacteria. *Appl Environ Microbiol* 74:2441–2446.
9. Salieb-Beugelaar GB, Simone G, Arora A, Philippi A, Manz A (2010) Latest developments in microfluidic cell biology and analysis systems. *Anal Chem* 82:4848–4864.
10. Krishnan M, Mojarad N, Kukura P, Sandoghdar V (2010) Geometry-induced electrostatic trapping of nanometric objects in a fluid. *Nature* 467:692–695.
11. Park S, Zhang Y, Wang TH, Yang S (2011) Continuous dielectrophoretic bacterial separation and concentration from physiological media of high conductivity. *Lab Chip* 11:2893–2900.
12. Takayama S, et al. (2001) Laminar flows: Subcellular positioning of small molecules. *Nature* 411:1016.
13. Liu YJ, et al. (2011) Surface acoustic wave driven light shutters using polymer-dispersed liquid crystals. *Adv Mater* 23:1656–1659.
14. Shi J, Ahmed D, Mao X, Lin SS, Huang TJ (2009) Acoustic tweezers: Patterning cells and microparticles using standing surface acoustic waves (SSAW). *Lab Chip* 9:2890–2895.
15. Woodside SM, Bowen BD, Piret JM (1997) Measurement of ultrasonic forces for particle-liquid separations. *AIChE J* 43:1727–1736.
16. Wang K, Schonbrun E, Steinvurzel P, Crozier KB (2011) Trapping and rotating nanoparticles using a plasmonic nano-tweezer with an integrated heat sink. *Nat Commun* 2:469.
17. Snezhko A, Aranson IS (2011) Magnetic manipulation of self-assembled colloidal asters. *Nat Mater* 10:698–703.
18. Manosas M, Spiering M, Zhuang Z, Benkovic SJ, Croquette V (2009) Coupling DNA unwinding activity with primer synthesis in the bacteriophage T4 primosome. *Nat Chem Biol* 5:904–912.
19. Khademhosseini A, May MH, Sefton MV (2005) Conformal coating of mammalian cells immobilized onto magnetically driven beads. *Tissue Eng* 11:1797–1806.
20. Chiou P-Y, Ohta AT, Wu MC (2005) Massively parallel manipulation of single cells and microparticles using optical images. *Nature* 436:370–372.
21. Jamshidi A, et al. (2008) Dynamic manipulation and separation of individual semiconducting and metallic nanowires. *Nat Photonics* 2:86–89.
22. Hsu H-Y, et al. (2010) Phototransistor-based optoelectronic tweezers for dynamic cell manipulation in cell culture media. *Lab Chip* 10:165–172.
23. Voldman JTJ (2006) Electrical forces for microscale cell manipulation. *Annu Rev Biomed Eng* 8:425–454.
24. Friend J, Yeo L (2011) Microscale acoustofluidics: Microfluidics driven via acoustics and ultrasonics. *Rev Mod Phys* 83:647–704.
25. Lenshof A, Laurell T (2010) Continuous separation of cells and particles in microfluidic systems. *Chem Soc Rev* 39:1203–1217.
26. Shi J, Mao X, Ahmed D, Colletti A, Huang TJ (2008) Focusing microparticles in a microfluidic channel with standing surface acoustic waves (SSAW). *Lab Chip* 8:221–223.
27. Schneider SW, et al. (2007) Shear-induced unfolding triggers adhesion of von Willebrand factor fibers. *Proc Natl Acad Sci USA* 104:7899–7903.
28. Franke T, Braunmüller S, Schmid L, Wixforth A, Weitz DA (2010) Surface acoustic wave actuated cell sorting (SAWACS). *Lab Chip* 10:789–794.
29. Lee J, et al. (2011) Targeted cell immobilization by ultrasound microbeam. *Biotechnol Bioeng* 108:1643–1650.
30. Manneberg O, Vanherberghen B, Önfelt B, Wiklund M (2009) Flow-free transport of cells in microchannels by frequency-modulated ultrasound. *Lab Chip* 9:833–837.
31. Vanherberghen B, et al. (2010) Ultrasound-controlled cell aggregation in a multi-well chip. *Lab Chip* 10:2727–2732.
32. Rezk AR, Qi A, Friend JR, Li WH, Yeo LY (2012) Uniform mixing in paper-based microfluidic systems using surface acoustic waves. *Lab Chip* 12:773–779.
33. Shi J, et al. (2011) Three-dimensional continuous particle focusing in a microfluidic channel via standing surface acoustic waves (SSAW). *Lab Chip* 11:2319–2324.
34. Shi J, et al. (2009) Continuous particle separation in a microfluidic channel via standing surface acoustic waves (SSAW). *Lab Chip* 9:3354–3359.
35. Frommelt T, et al. (2008) Microfluidic mixing via acoustically driven chaotic advection. *Phys Rev Lett* 100:1–4.
36. Wiklund M, et al. (2006) Ultrasonic standing wave manipulation technology integrated into a dielectrophoretic chip. *Lab Chip* 6:1537–1544.
37. Vanherberghen B, et al. (2010) Ultrasound-controlled cell aggregation in a multi-well chip. *Lab Chip* 10:2727–2732.
38. Bruus H (2011) Acoustofluidics 1: Governing equations in microfluidics. *Lab Chip* 11:3742–3751.
39. Lenshof A, Evander M, Laurell T, Nilsson J (2012) Acoustofluidics 5: Building microfluidic acoustic resonators. *Lab Chip* 12:684–695.
40. Dual J, Hahn P, Leibacher I, Möller D, Schwarz T (2012) Acoustofluidics 6: Experimental characterization of ultrasonic particle manipulation devices. *Lab Chip* 12:852–862.
41. Bruus H (2012) Acoustofluidics 7: The acoustic radiation force on small particles. *Lab Chip* 12:1014–1021.
42. Lenshof A, Magnusson C, Laurell T (2012) Acoustofluidics 8: Applications of acoustophoresis in continuous flow microsystems. *Lab Chip* 12:1210–1223.
43. Glynne-Jones P, Boltryk RJ, Hill M (2012) Acoustofluidics 9: Modelling and applications of planar resonant devices for acoustic particle manipulation. *Lab Chip* 12:1417–1426.
44. Chung K, Crane MM, Lu H (2008) Automated on-chip rapid microscopy, phenotyping and sorting of *C. elegans*. *Nat Methods* 5:637–643.
45. Campbell CK (1998) *Surface Acoustic Wave Devices for Mobile and Wireless Communications* (Academic Press, Orlando), pp 217–220.
46. Neuman KC, Nagy A (2008) Single-molecule force spectroscopy: Optical tweezers, magnetic tweezers and atomic force microscopy. *Nat Methods* 5:491–505.